Post-synthesis stabilization of germanosilicate zeolites ITH, IWW and UTL by substitution of Ge for Al

Mariya V. Shamzhy,[a*] Pavla Eliašová,[b] Dana Vitvarová,[a] Maksym V. Opanasenko,[b] Daniel S. Firth,[c] Russell E. Morris[c]

Abstract: Germanosilicate zeolites often suffer from low hydrothermal stability due to the high content of Ge. Here we investigated the post-synthesis introduction of Al accompanied with stabilization of selected germanosilicates by degermanation/alumination treatments. The influence of chemical composition and topology of parent germanosilicate zeolites (**ITH**, **IWW** and **UTL**) on the post-synthesis incorporation of Al was studied. Alumination of **ITH** (Si/Ge = 2 – 13) and **IWW** (Si/Ge = 3 – 7) zeolites resulted in the partial substitution of Ge for Al (up to 80 %) enhancing with decrease Ge content in the parent zeolite. In contrast, in extra-large pore zeolite **UTL** (Si/Ge = 4 – 6) the hydrolysis of the interlayer Ge–O bonds dominated over substitution. The stabilization of zeolite **UTL** was achieved using novel 2-step degermanation/alumination procedure by the partial post-synthesis substitution of Ge for Si followed by alumination. This new method of stabilization and incorporation of strong acid sites may extend the utilization of germanosilicate zeolites, which has been until now limited.

Introduction

During the last decade germanosilicate zeolites have attracted a lot of attention. Germanium acts as an inorganic structure-directing agent (SDA) with a particular selectivity towards frameworks containing Ge-enriched double-four-ring (D4R) units.[1] The stabilization of small-rings by Ge has allowed for the synthesis of many new structures such as **BEC**,[1a, 2] **ASV**,[3] **IWR**,[4] **IWS**,[5] **IWW**,[6] **IRR**,[1e] **–ITV**,[7] **UTL**,[8] **ITR**,[9] **UWY**[10] etc. The hydrolytic instability of Si–O–Ge and Ge–O–Ge linkages, combined with the regioselective location of Ge atoms in D4R units,[11] has enabled the development of a new top-down strategy. The selective disassembly of germanosilicates like **UTL**[12] and **IWW**,[13] containing unidirectional hydrolytically unstable D4R units, has allowed the formation of new layered zeolitic materials. In contrast the hydrolysis of frameworks containing Ge-enriched D4Rs in three directions (e.g. **BEC**,[1a] **IWS**,[5] **IRR**,[1e] **STW**,[14] etc.) results in full fragmentation, even in ambient air moisture.

Due to the presence of small structural units (e.g. D4R, D3R) the frameworks of germanosilicates are generally characterized by low densities (up to 10.5 T/1000 Å^3) and high pore volumes (accessible volume up to 40 %), making them especially suitable in processing bulky molecules.[1c] However, the low hydrothermal stability and high cost of Ge significantly limits the practical use of Ge-containing zeolites.

The post-synthesis replacement of framework cations, commonly applied to calcined SDA-free zeolites, is frequently not acceptable for germanosilicate zeolites, due to their inability to withstand high temperature treatment. Thus, the post-synthesis stabilization of SDA-containing germanosilicate zeolites was attempted. It has been reported that, under low acidic conditions, aluminium could be incorporated into the **BEC** (Si/Ge = 3.6) framework with the simultaneous removal of Ge and SDA.[15] The substitution of Ge for Si under highly acidic conditions was recently reported for as-synthesized **IWW**,[16] **IWR**, **BEC**, **UWY** and **UTL**[17] zeolites. Previously we reported new approaches to tune the strength of acid sites through the post-synthesis treatment of **IWR** and **ITH** zeolites.[18]

To the best of our knowledge, the stabilization and functionalization of the extra-large pore zeolite **UTL**, through the post-synthesis incorporation of aluminium, has not been examined. Moreover, up-to-now post-synthesis introduction of acid centers to the frameworks of **IWW** and **ITH** zeolites was succeeded only for a limited chemical compositions – using Ge-poor samples for former case and Ge-rich samples for latter zeolite. Therefore, in this contribution we assess the influence of crucial parameters of parent materials (framework type, chemical composition, presence of the SDA in the channels, etc.) and treatment conditions on the stability and the extent of Ge for Al substitution in **UTL, ITH, IWW** zeolites of different Ge-content.

Results and Discussion

Parent germanosilicate zeolites

The topologies of zeolites **ITH**, **IWW**, **UTL** are similar as they can all be viewed as dense two-dimensional (2D) layers separated by D4R bridging units enriched with Ge (Figure 1). Ge atoms (almost 95 %) were found to preferentially occupy T sites within the D4R units of **UTL**,[8] **IWW**[19] and Ge-poor (Si/Ge > 5) **ITH**.[20] Ge-rich **ITH** also has up to 50 % Ge occupation in the [$4^1 5^2 6^2$] cages in the layers.[20-21] The chemical composition of **UTL** prepared from reaction mixtures with different Si/Ge molar ratio was found to vary between 3.8 – 6.7.[8, 22] The molar ratio Si/Ge = 4.5 corresponds to 7 Ge atoms per D4R unit (7Ge,1Si).[8a] With a higher Si/Ge molar ratio (Si/Ge = 6.7) the average number of Ge atoms decreases to 5 per D4R unit

[a] Dr. Mariya V. Shamzhy, Dr. Dana Vitvarová
Department Synthesis and Catalysis
J. Heyrovský Institute of Physical Chemistry of the Czech Academy of Sciences, v. v. i.
Dolejškova 3, CZ-182 23 Prague 8, Czech Republic
E-mail: mariya.shamzhy@jh-inst.cas.cz
[b] Dr. Pavla Eliašová, Dr. Maksym V. Opanasenko
Department of Physical and Macromolecular Chemistry, Faculty of Science
Charles University in Prague
Hlavova 2030, 12840 Prague 2, Czech Republic
[c] Daniel S. Firth, Prof. Russell E. Morris
EaStCHEM School of Chemistry
University of St. Andrews
St. Andrews KY16 9ST (UK)

Supporting information for this article is given via a link at the end of the document.

(5Ge,3Si). Upon the hydrolysis of Ge-rich **UTL** (Si/Ge = 5.1) only a narrow signal ca. ~-10 ppm in the ^{19}F NMR spectrum was observed. This indicated the exclusive formation of $(SiO)_3SiOH$ and the presence of one germanate four-ring in each D4R unit (4Ge,4Si) in the parent germanosilicate.[23]

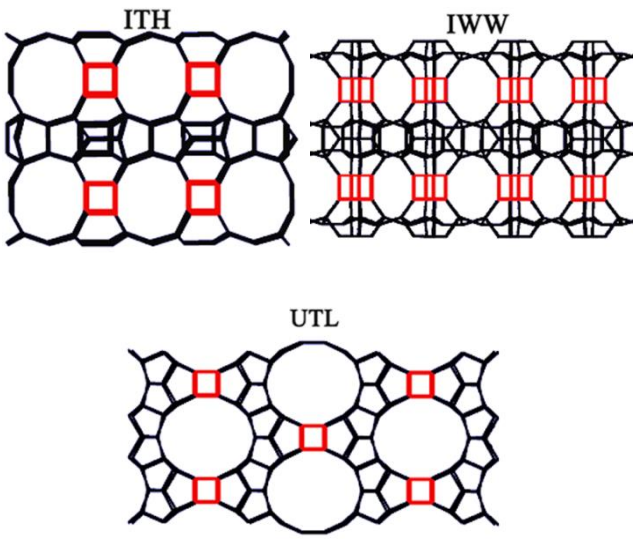

Figure 1. Structure of zeolites **ITH** (010 projection), **IWW** (010 projection), **UTL** (001 projection).

In order to vary the chemical composition of parent materials, we prepared a series of **UTL**, **IWW** and **ITH** zeolites including their Ge-poor and Ge-rich forms (Table 1). Ge-rich zeolites had Si/Ge ratios in the range 2.3 – 3.8, while Ge-poor samples were characterized by Si/Ge ratios 6.0 – 13.3. XRD patterns of all as-synthesized samples matched well with those reported in the literature indicating a high degree of crystallinity and phase purity (Figure S1, Supporting information).

Table 1. Chemical composition and textural properties of parent germanosilicates.

Sample	Chemical composition,mol. %		Si/Ge	Crystal size (μm)	V_{micro}, $cm^3 \cdot g^{-1}$	V_{total}, $cm^3 \cdot g^{-1}$
	Si	Ge				
ITH-13	93.0	7.0	13.3	5 x 0.5 x 0.5	0.12	0.20
ITH-2	69.7	30.3	2.3	15 x 1 x 0.5	0.13	0.18
IWW-7	87.8	12.2	7.2	0.5–1	0.16	0.30
IWW-3	74.4	25.6	2.9	0.5–1	0.17	0.30
UTL-6	85.7	14.3	6.0	25 x 20 x 0.1	0.21	0.24
UTL-4	79.1	20.8	3.8	30 x 20 x 0.1	0.19	0.20

All zeolites under investigation exhibit a type I isotherm in gas adsorption experiments (Figure S2, Supporting information) with a steep increase in the amount adsorbed at low relative pressures (p/p_0 < 0.01) indicating filling of the micropores. The micropore volumes decreased in the order: **UTL** (0.19 – 0.21 $cm^3 \cdot g^{-1}$) > **IWW** (0.16 – 0.17 $cm^3 \cdot g^{-1}$) > **ITH** (0.12 – 0.13 $cm^3 \cdot g^{-1}$) (Table 1) reflecting the different pore dimensions of the zeolites: 14-12-ring (**UTL**) > 12-10-8-ring (**IWW**) > 10-10-9-ring (**ITH**).

ITH zeolite formed platelet-like crystals (Figure 2A and B) in which the sinusoidal 10-R channel goes along the c-axis with a length of 5 – 15 μm (Table 1), whereas the other 10- and the 9-R channels occur along the *a*–*b* plane (0.5 – 1 μm, Table 1).[24] In contrast, **IWW** showed small crystals between 0.5 – 1 μm crystallizing in agglomerates (Figure 2C and D). **UTL** zeolites formed quite uniform thin rectangular crystals in which 12- and 14-R channels occur along *b*–*c* plane (25 – 30 x 20 μm, Table 1), while the shortest dimension of the crystal (0.1 μm, Table 1) goes along *a* axis (Figure 2E and F).[25]

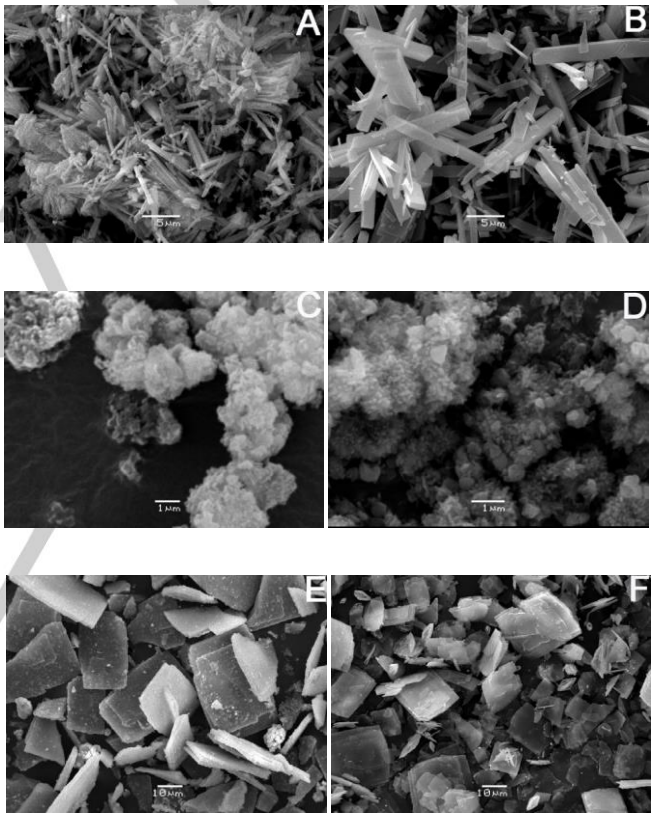

Figure 2. SEM images of germanosilicate zeolites: *ITH-13* (**A**), *ITH-2* (**B**), *IWW-7* (**C**), *IWW-3* (**D**), *UTL-6* (**E**), and *UTL-4* (**F**).

Although thermally stable germanosilicates under investigation demonstrated a low hydrolytic stability: only Ge-poor **ITH** and **IWW** zeolites maintained the structural ordering upon the treatment with 0.01 M HNO_3 at pH = 2 (Figure 3) corresponding to the standard post-synthesis substitution of Ge for Al procedure (e.g. the treatment of calcined zeolite with 1 M $Al(NO_3)_3$ solution (pH = 2) at 80 °C for 24 h)[26]. This method of alumination was chosen as a basic treatment approach since it is performed under conditions preventing mobility of framework Si atoms due to formation of either cationic or anionic species (isoelectric point of silica lies in the range pH = 1.5 – 3.5).[27] The results of alumination indicated that Al prevents the destruction

of Ge-rich **ITH** and **IWW** frameworks in acidic medium (Figure 3). Ge-rich **ITH** and **IWW** zeolites subjected to alumination showed a drop in Ge concentration while maintaining their structure ordering despite the treatment at pH = 2.

Incorporated Al generated both Brønsted and Lewis acid sites in *calcITH/Al* and *calcIWW/Al* (*vide infra*). However the presence of Al in the medium did not increase the hydrolytic stability of **UTL**, which was destroyed during the alumination treatment (Figure 3C).

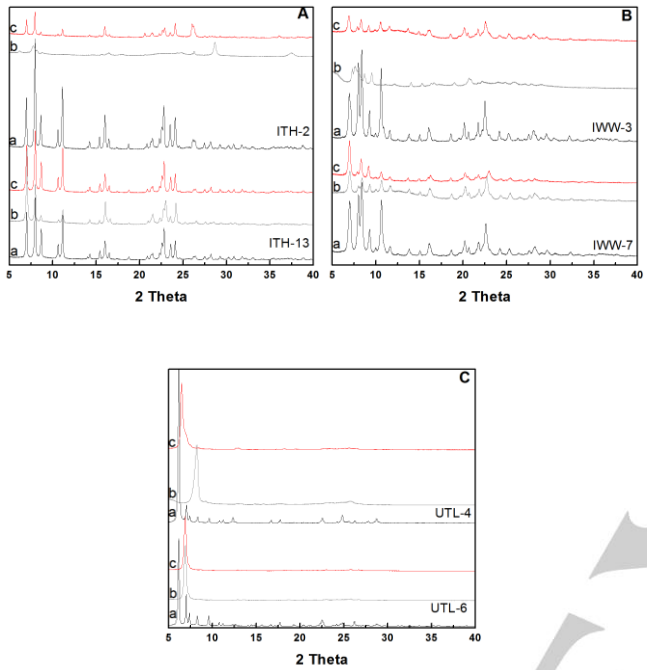

Figure 3. XRD patterns of **ITH** (**A**), **IWW** (**B**), **UTL** (**C**): calcined zeolites (a), zeolites treated with 0.01 M HNO_3 solution at T = 25 °C for τ = 24 h (b), *calcZeolite/Al* (c).

We hypothesize two reasons for the lack of **UTL** stabilization *via* the standard alumination technique. 1) The critically lower rate of $Al(H_2O)_6^{3+}$ diffusion *vs.* degermanation in the channels occurring along *b*–*c* plane of the crystals (25 – 30 x 20 µm, Table 1). 2) The specific arrangement of Ge in the D4Rs of **UTL** (i.e. the presence of a Ge-pure S4R units within D4Rs[23]). This restricts the substitution of Ge for Al. In contrast, diffusion limitations do not seem to limit the substitution of Ge for Al in **ITH** and **IWW** (*vide infra*). Both formed tiny crystals (Figure 2 A–D, Table 1) and are characterized by three-dimensional pore systems.

Therefore, a set of modified alumination procedures were attempted for **UTL**. As-synthesized SDA-containing **UTL** was used in three different procedures: a one-step post-synthesis alumination with $Al(NO_3)_3$ (Scheme 1, procedure 3) and a two-step substitution *via* consecutive degermanation/alumination in TEOS-free (Scheme 1, procedure 4) and TEOS-containing mixtures (Scheme 1, procedure 5). The latter technique was also applied for calcined zeolites (Scheme 1, procedure 2). The idea to use SDA-containing zeolites as starting materials was based on the possible stabilization of the zeolite framework by organic molecules occluded in the pores, previously shown for **BEC**.[15, 28] TEOS was intentionally used to stabilize the D4Rs by their enrichment with Si. To address the influence of zeolite topology and chemical composition on the outcome of post-synthesis Al incorporation, we also applied the modified alumination procedures to the other germanosilicates under investigation.

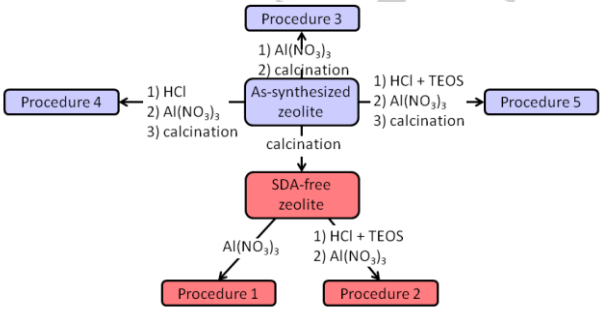

Scheme 1. Post-synthesis alumination of germanosilicate zeolites: procedures.

Post-synthesis treatment

As-synthesized UTL zeolites. The treatment of SDA-containing **UTL** with $Al(NO_3)_3$ solution (pH = 2, procedure 3, Scheme 1) did not cause any structural transformation of the framework (Figure 4). However the prepared *asUTL/Al* samples showed a relatively low degree of degermanation and no Al incorporation. EDX analysis showed a slight increase in Si/Ge from 6.0 to 6.2 and 3.8 to 5.1 for Ge-poor and Ge-rich **UTL** respectively (Table S2, Supporting information).

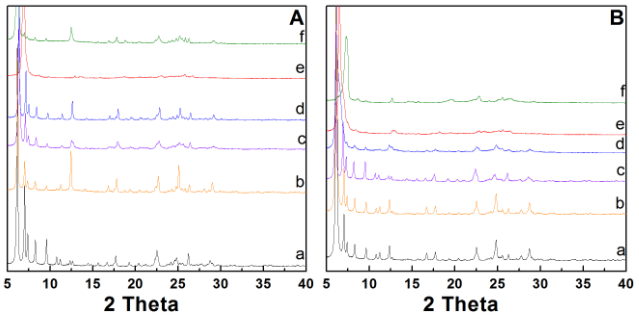

Figure 4. XRD patterns of *UTL-6* (**A**) and *UTL-4* (**B**): calcined zeolites (a), *asUTL/Al/calc* (b), *asUTL/HCl/Al/calc* (c), *asUTL/HCl+TEOS/Al/calc* (d), *calcUTL/Al* (e), *calcUTL/HCl+TEOS/Al* (f).

asUTL/Al/calc samples showed a similar concentration of silanol groups (absorption band at 3745 cm^{-1} in FTIR spectra, Figure 5) as the parent **UTL** zeolite. The treatment of SDA-containing **UTL** with a 1 M HCl solution under hydrothermal conditions led to a twofold increase in the Si/Ge ratios for both Ge-poor (Si/Ge = 11.8 and 6 for *asUTL-6/HCl/Al/calc* and *UTL-6/calc*, respectively) and Ge-rich **UTL** (Si/Ge = 10.3 and 3.8 for *asUTL-4/HCl/Al/calc* and *UTL-4/calc*, respectively). With analysis showing an increase in the intensity of the absorption band at 3745 cm^{-1} in FTIR spectra (Figure 5). These results indicate a partial extraction of Ge atoms (i.e. breaking of unstable Si–O–Ge linkages) from the SDA-containing germanosilicate zeolites under acidic conditions. XRD analysis confirmed the

preservation of the structure of *asUTL-6/HCl* (Figure S3, Supporting information) and the collapse of the *asUTL-4/HCl* framework. This was due to the higher number of Ge atoms present in the framework, which have to be replaced by Si from the partial dissolution of the dense layers at pH ≈ 0[17, 29] to maintain the structural ordering of **UTL**. By introducing an additional silica source at highly-acidic medium during the degermanation step we were able to preserve the *UTL-4* framework (Figure S3, Supporting information), while increasing the Si/Ge ratio from 3.8 to 7.0 when compared with the parent zeolite (Table S2, Supporting information). This was confirmed by FTIR as degermanated *asUTL* samples in the presence of TEOS showed a lower concentration of silanol groups than *asUTL/HCl/Al/calc* (Figure 5).

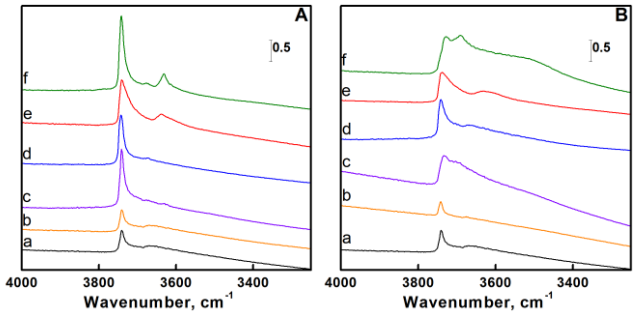

Figure 5. FTIR spectra of *UTL-6* (**A**) and *UTL-4* (**B**) zeolites in region of hydroxyl vibrations: calcined zeolites (a), *asUTL/Al/calc* (b), *asUTL/HCl/Al/calc* (c), *asUTL/HCl+TEOS/Al/calc* (d), *calcUTL/Al* (e), *calcUTL/HCl+TEOS/Al* (f).

Further alumination of *asUTL-6/HCl*, *asUTL-6/HCl+TEOS* and *asUTL-4/HCl+TEOS* did not cause any decrease in the crystallinity of samples (Figure S3, Supporting information). However only a small amount of Al generating Brønsted and Lewis acid centers were incorporated in *asUTL-6* when degermanated with hydrochloric acid (62 μmol g^{-1}, Table S2, Supporting information). No Al was found in *asUTL-6/HCl+TEOS/Al/calc.* This result may be connected with preferential healing of silanol nests with Si in the presence of TEOS.

SDA-free UTL zeolites. To increase access to the entire volume of **UTL** by the substituting ion and to overcome the restrictions imposed on the substitution of Ge for Al by the presence of Ge–O–Ge bonds in D4R units we attempted the consecutive degermanation of an SDA-free zeolite in the presence of a Si source, to initiate partial substitution of Ge for Si, followed by alumination (Scheme 1, procedure 2). It was found that, unlike SDA-containing *UTL-4* zeolite, treatment of calcined *UTL-4* with an ethanolic HCl/TEOS mixture, followed by alumination resulted in the destruction of the zeolite framework (Figure 4 and Figure S4, Supporting information). The maintenance of the *asUTL-4* framework after treatment with the HCl/TEOS mixture may be due to the presence of SDA cations, which causes a deceleration in the hydrolysis of Ge–O bonds. Indeed the *asUTL-4/HCl+TEOS/Al* sample showed a remarkably lower drop in Ge concentration (40 % of Ge leached, Table S2, Supporting information) in comparison to *calcUTL-4/HCl+TEOS/Al* (87 % of Ge leached, Table S2, Supporting information).

In contrast to two-step degermanation/alumination of Ge-rich *UTL-4,* the *calcUTL-6/HCl+TEOS/Al* sample showed the preservation of the structure under similar degermanation/alumination conditions (Figure 4 and Figure S4, Supporting information). This may indicate the different rates of degermanation and substitution in Ge-poor samples.

^{27}Al MAS NMR spectrum of *calcUTL-6/HCl+TEOS/Al* showed a dominant peak at 50 – 80 ppm (Figure 6). This confirmed the incorporation of Al into the framework positions of **UTL**.[30] The introduction of Al resulted in generation of both Brønsted (222 μmol g^{-1}) and Lewis (364 μmol g^{-1}) acid sites in *calcUTL-6/HCl+TEOS/Al* (Table 2).

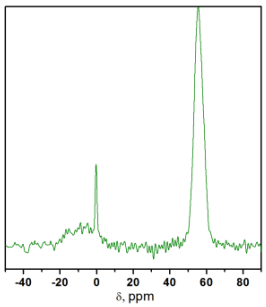

Figure 6. ^{27}Al MAS NMR spectra of *calcUTL/HCl+TEOS/Al.*

Ar adsorption (Figure 7) showed a decrease in the micropore volume (0.14 *vs.* 0.21 $cm^3 \cdot g^{-1}$, Table 2) with a simultaneous enhancement of total pore volume (0.36 *vs.* 0.24 $cm^3 \cdot g^{-1}$, Table 2) in *calcUTL-6/HCl+TEOS/Al vs. UTL-6*. Also *calcUTL-6/HCl+TEOS/Al* showed the same micropore size distribution centered at 0.65 nm as original the *UTL-6* zeolite, with an additional broad size distribution of large mesopores (Figure 7B). The presence of large mesopores and macropores in *calcUTL-6/HCl+TEOS/Al* is most likely connected with formation of intercrystalline linkages, through the partial deposition of extra-framework silica and the non-equivalent replacement of leached Ge for Si/Al atoms, in the course of post-synthesis degermanation/alumination.

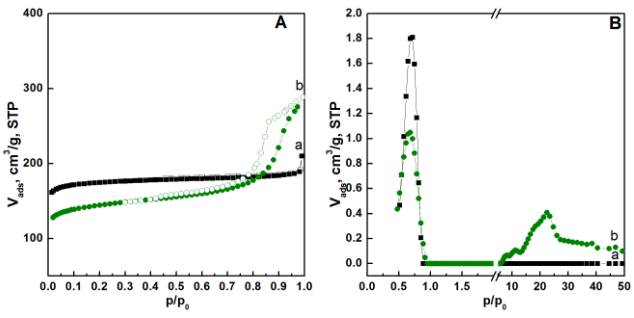

Figure 7. Argon adsorption (•) and desorption (○) isotherms (**A**) and pore-size distribution (**B**) of *UTL-6* (a) and *calcUTL-6/HCl+TEOS/Al* (b) zeolites.

Substitution of Ge for Si/Al in *calcUTL-6/HCl+TEOS/Al* leads to an enhancement of the hydrolytic stability of the UTL framework. In contrast to *UTL-6*, the treatment of *calcUTL-*

Table 2. Chemical composition, textural and acidic properties of aluminated **ITH**, **IWW** and **UTL** zeolites.

Sample	V_{micro}, $cm^3 \cdot g^{-1}$	V_{total}, $cm^3 \cdot g^{-1}$	Chemical composition		Al_{Th}[a], mol. %	Δw[b], %	Concentration of acid sites, $\mu mol\ g^{-1}$		
			Al, mol. %	Si/Ge			C_B	C_L	C_Σ
ITH-13	0.12	0.20	–	13	–	–	–	–	–
calcITH-13/Al	0.14	0.32	2.0	20	1.8	4	51	160	211
calcITH-13/HCl+TEOS/Al	0.05	0.11	–	17	–	3	–	–	–
ITH-2	0.13	0.18	–	2	–	–	–	–	–
calcITH-2/Al	0.13	0.25	1.5	13	1.3	16	68	262	330
calcITH-2/HCl+TEOS/Al	0.02	0.04	–	5	–	10	–	–	–
IWW-7	0.16	0.30	–	7	–	–	–	–	–
calcIWW-7/Al	0.19	0.39	7.6	36	6.4	9	346	411	757
calcIWW-7/HCl+TEOS/Al	0.09	0.46	5.0	20	4.4	7	211	320	533
IWW-3	0.17	0.30	–	3	–	–	–	–	–
calcIWW-3/Al	0.18	0.52	7.1	21	6.1	15	284	427	711
calcIWW-3/HCl+TEOS/Al	0.14	0.39	4.8	19	4.2	17	242	274	516
UTL-6	0.21	0.24	–	6	–	–	–	–	–
calcUTL-6/HCl+TEOS/Al	0.14	0.36	5.7	39	5.4	11	222	364	586

[a] calculated based on the integral intensities of peaks at 0 and 60 ppm in ^{27}Al NMR spectra

[b] weight reduction after alumination [m (parent) – m (aluminated)] / m (parent) • 100 %

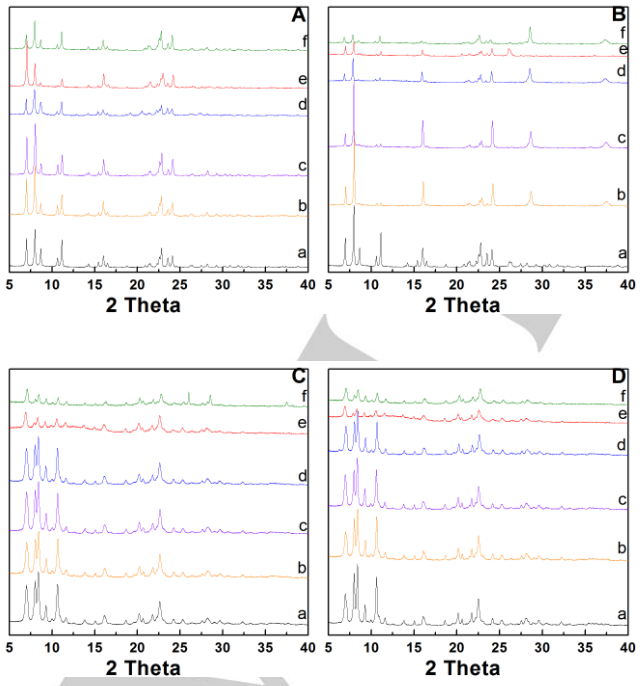

Figure 8. XRD patterns of *ITH-13* (**A**), *ITH-2* (**B**), *IWW-7* (**C**), *IWW-3* (**D**): calcined zeolites (a), *asZeolite/Al/calc* (b), *asZeolite/HCl/Al/calc* (c), *asZeolite/HCl+TEOS/Al/calc* (d), *calcZeolite/Al* (e), *calcZeolite/HCl+TEOS/Al* (f).

6/HCl+TEOS/Al with water did not cause any structural transformation of the zeolite (Figure S5, Supporting information). This is consistent with the lower reactivity of Si–O–Si and Si–O–Al *vs.* Si–O–Ge bonds.[31]

As-synthesized ITH and IWW zeolites. XRD patterns of **ITH** and **IWW** subjected to the 1-step alumination or 2-step degermanation/alumination procedures (Figure 8) showed diffraction lines with slightly decreased intensities at the characteristic 2 theta positions. This indicated the preservation of the structural ordering of the respective zeolites with a decrease in framework density due to the leaching of Ge atoms (Table S1, Supporting information). The appearance of additional diffraction lines at 20.6 and 26.1 – 27 ° in the XRD pattern of Ge-rich **ITH**, when treated in the as-synthesized form or when degermanated in ethanolic HCl solution, was attributed to a crystalline phase of GeO_2.

Similarly to **UTL**, post-synthesis treatment of SDA-containing **ITH** and **IWW** did not result in a substantial change in the Si/Ge ratio (Table S1, Supporting information). Thus, slightly acidic environments seem to be inappropriate for the deep degermanation of SDA-containing zeolites with a 1-dimensional location of Ge-enriched domains.

In contrast to the medium-pore zeolite **ITH** (Figure 2A and B), alumination of *asIWW* zeolites was less hindered by crystal size (Figure 2C, D) and led to the formation of acid centres. However these were in limited amounts (17 – 59 $\mu mol\ g^{-1}$) when compared with the post-synthesis treatment of SDA-free zeolites (516 – 757 $\mu mol\ g^{-1}$, Table S1, Supporting information). The

characteristics of modified SDA-free germanosilicates is discussed in details *vide infra*.

SDA-free ITH and IWW zeolites. ^{27}Al MAS NMR spectra of *calcITH/Al* and *calcIWW/Al* samples (Figure S6, Supporting information) show the dominating peak (shift ranges of 50 – 80 ppm) corresponding to the framework tetrahedral AlO_4 species and a smaller peak (-10 – 15 ppm) assigned to octahedral AlO_6 extra-framework species. The increased absorption band at 3745 cm^{-1} in the FTIR spectra of *calcZeolite/Al* with respect to the parent germanosilicate (Figure S7, Supporting information) agrees with the breaking of the hydrolytically unstable Si–O–Ge linkages and the formation of a non-equivalent amount of bridging Si–O–Al bonds (absorption band at 3620 cm^{-1}, Figure S7, Supporting information).

Ge-rich *ITH-2* has Ge atoms located both in the D4R units and $[4^15^26^2]$ cages[20, 32] and showed a greater loss of Ge than Ge-poor *ITH-13* (77 % *vs* 33 % respectively) during the post-synthesis alumination (Table 2). This may be connected with a more rapid leaching of Ge atoms from the $[4^15^26^2]$ intralayer cages in comparison to the D4Rs. As the location of the $[4^15^26^2]$ intralayer cages, at the intersection of 9- and 10-ring pores, makes them more accessible than the D4Rs, which are only accessible from the 10-ring channels of **ITH**.

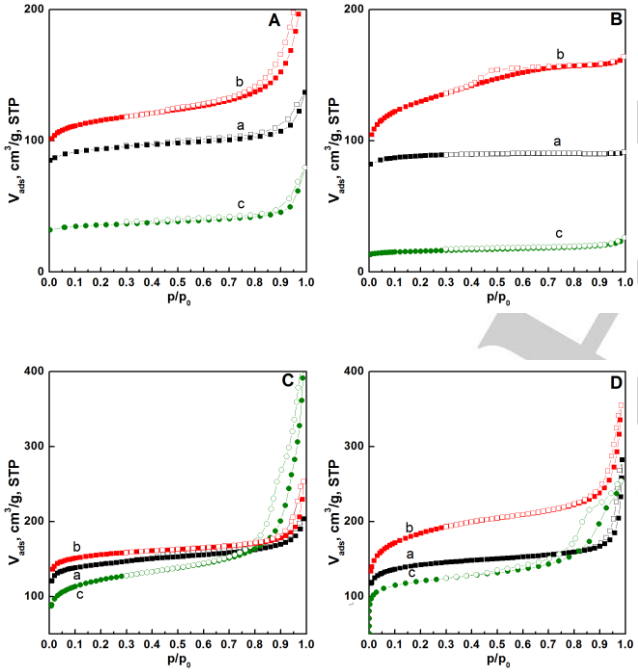

Figure 9. Nitrogen adsorption (•) and desorption (○) isotherms of *ITH-13* (**A**), *ITH-2* (**B**), *IWW-7* (**C**) and *IWW-3* (**D**): calcined zeolites (a), *calcZeolite/Al* (b), *calcZeolite/HCl+TEOS/Al* (c).

The decrease in the Ge content of aluminated *ITH-13* (by 2.3 mol. % in *calcITH-13/Al*) and *IWW-7* (by 9.7 mol. % in *calcIWW-7/Al*) roughly corresponds to the amount of incorporated Al (1.8 mol. % for *calcITH-13/Al* and 6.8 mol. % for *calcIWW-7/Al* (Table 2)). In contrast to Ge-poor *ITH-13* and *IWW-7* zeolites, the amount of Ge extracted from *ITH-2* (19.0 mol. %) and *IWW-3* (21.4 mol. %) samples remarkably exceeded the concentration of the incorporated Al (1.3 – 6.5 mol. %, Table 2). Despite the inconsistency in the amount of extracted/incorporated framework atoms, XRD data indicated the maintenance of interlayer bonds and structural ordering of Ge-rich *IWW-3* and *ITH-2* after alumination. In the absence of Al, a full breaking of interlayer linkages took place under similar conditions (Figure 3B).

In contrast to *IWW-3*, Ge-poor *IWW-7* showed the total substitution of Ge for Al. *IWW-7* possesses D4R units containing 4 Ge,[13] evenly distributed to avoid the formation of Ge–O–Ge bonds. Thus Ge-poor **IWW** materials were unaffected by the Löwenstein rule during the alumination procedure.[33] Chemical analysis showed that about 70 % of Ge leached from *IWW-7* samples was substituted with Al atoms in *calIWW-7/Al* (Table 2), enabling the maintenance of interlayer linkages.

Ge-poor *calcITH-13/Al* and *calcIWW-7/Al* exhibited type I adsorption/desorption isotherms similar to their parent zeolites, but had a higher uptake in the range of filling micropores (Figure 9A and C). Ge-rich *calcZeolite/Al* samples were characterized by an increase in both the micropore and mesopore volumes (Table 2). The formation of mesopores is assumed to be connected with the higher degree of degermanation in Ge-rich samples and the non-equivalent replacement of leached Ge for Si/Al (Table 2). Such development of mesoporosity during alumination of the samples with high content of Ge can be considered as advantage of the proposed method since it allows not only to incorporate reasonable amount of potential active sites, but also to create additional transport pores usually facilitating catalytic transformation of bulk molecules.[34]

Noticeably, *calcZeolite/HCl+TEOS/Al* samples prepared using a 2-step degermanation/alumination treatment (Scheme 1, procedure 2) showed lower adsorption characteristics (Table 2) in comparison with *calcZeolite/Al* zeolites (Scheme 1, procedure 1). For *calcITH-2/HCl+TEOS/Al* there was a significant drop in micropore volume (V_{micro} = 0.02 $cm^3 \cdot g^{-1}$) in comparison with *calcITH-2/Al* (V_{micro} = 0.13 $cm^3 \cdot g^{-1}$, Table 2, *vide infra*) that may be connected to the undesired deposition of silica/GeO_2 in the relatively narrow pores of **ITH**. This phenomenon is less pronounced for large-pore **IWW** and especially extra-large-pore **UTL** zeolites subjected to 2-step alumination procedure using TEOS (Table 2). The results also show the slower rate of diffusion for Ge-containing species leached from medium-pore **ITH** in ethanolic *vs.* aqueous medium. Similarly to *calcUTL-6/HCl+TEOS/Al*, **IWW** samples prepared using a 2-step degermanation/alumination treatment (Scheme 1, procedure 2) showed isotherms with a steep rise at $p/p_0 > 0.05$ (Figure 9C and D).

Alumination resulted in the generation of a remarkably high number of acid sites in large-pore *calcIWW/Al* (711 – 757 μmol g^{-1}, Table 2) *vs.* medium-pore *calcITH/Al* zeolites (211 – 330 μmol g^{-1}, Table 2). This is due to the lower efficiency of alumination for medium-pore zeolites as the inner pores are poorly accessible for bulky hydrated aluminium cations.[26] The decreased concentration of silanol defects (Figure S7, Supporting information) and lower amount of incorporated acid sites in *calcZeolite/HCl+TEOS/Al vs. calcZeolite/Al* (Table 2) is consistent with partial substitution of Si for Ge in *calcZeolite/HCl+TEOS/Al.*

Hydrothermal stability test showed the improved performance of aluminated *calcITH-2/Al*, *calcWW-3/Al*, *calcUTL-6/HCl+TEOS/Al* zeolites in comparison with parent germanosilicates destructing under hydrothermal conditions (Figure S8, Supporting information).

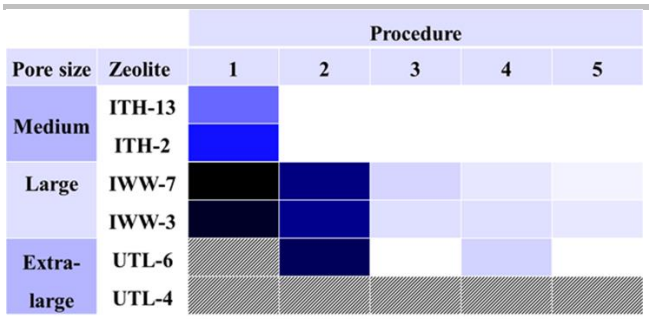

Scheme 2. Post-synthesis alumination of germanosilicate zeolites: acidity vs. characteristics of parent germanosilicates / treatment procedure (deeper color means higher concentration of formed acid centers, hatched areas correspond to samples collapsed upon treatment).

Catalytic performance of aluminated germanosilicates in tetrahydropyranylation of 1-propanol

The catalytic behavior of aluminated germanosilicate zeolites was investigated in a model reaction of 1-propanol tetrahydropyranylation. While negligible conversion of alcohol (2 – 5 % after 24 h) was observed over parent germanosilicate zeolites containing only a small amount of weak Lewis acid centres (Table 2), both *calcZeolite/Al* and *calcZeolite/HCl+TEOS/Al* samples showed the selective transformation of 1-propanol into the targeted tetrahydropyranyl ether (Figure 10).

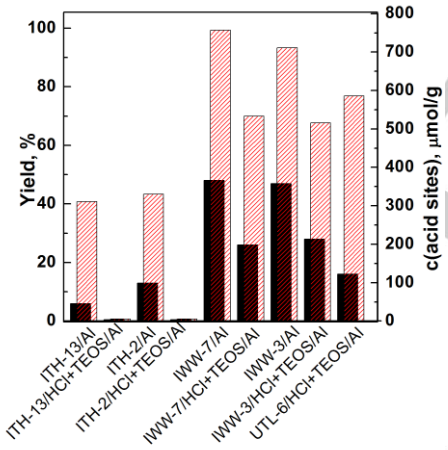

Figure 10. The yield of ether (■) formed after τ = 60 min in tetrahydropyranylation of 1-propanol over aluminated germanosilicate zeolites possessing (☑) acid sites.

In general, calcZeolite/Al zeolites possessing more acid centers showed higher yields in comparison with calcZeolite/HCl+TEOS/Al (Fig 10). For instance, the increase in the concentration of acid sites in *calcIWW-3/Al* (711 μmol g^{-1}) *vs. calcIWW-3/HCl+TEOS/Al* (516 μmol g^{-1}) was accompanied with enhancing yield from up to 47 % (Figure 10). Lower activity of *calcUTL-6/HCl+TEOS/Al vs. calcIWW/Al* zeolites having similar concentration of acid sites (516 – 533 μmol g^{-1}, Table 2) is consistent with larger size of crystals characteristic for **UTL** (Fig. 2, E) in which 12- and 14-R channels occurring along the longest dimensions (25 x 20 μm, Table 1), e.g. longer diffusion path of reacting molecules to the active centers. No conversion of 1-propanol was observed over *calcITH/HCl+TEOS/Al* samples having no incorporated acid sites (Table S1) and poor adsorption characteristics (Table 2).

Conclusions

The post-synthesis treatment of medium-pore **ITH** (Si/Ge = 2 – 13) and large-pore **IWW** (Si/Ge = 3 – 7) zeolites can be used to control the degree of Ge-to-Al substitution and textural properties of resulting materials by choosing the appropriate chemical composition of parent zeolite and alumination conditions. The amount of Ge extracted from Ge-rich **IWW** (Si/Ge = 3) drastically exceeded the concentration of incorporated Al (30 %), while 70 % – 78 % of the Ge leached from Ge-poor **IWW** (Si/Ge = 7) and **ITH** (Si/Ge = 13) was replaced with Al atoms. Alumination resulted in the generation of a significantly higher number of acid sites in large-pore **IWW** (711 – 757 μmol g^{-1}) compared to medium-pore **ITH** (211 – 330 μmol g^{-1}), indicating diffusion control of the alumination process (Scheme 2).

Conversely, in zeolite **UTL** (Si/Ge = 4 – 6) the hydrolysis of interlayer Ge–O bonds is typically dominated process and only the application of the modified 2-step degermanation/alumination treatment allowed the partial substitution of Ge for Al. The aluminated **UTL** not only preserved its structure, but in addition a remarkable amount of Brønsted (222 μmol g^{-1}) and Lewis (364 μmol g^{-1}) acidity was generated.

Non-equivalent exchange of Ge for Al in **ITH** (Si/Ge = 2), **IWW** (Si/Ge = 3) and **UTL** (Si/Ge = 6) allowed modification of textural characteristics of Ge-rich zeolites ended up forming hydrolytically stable hierarchical micro-mesoporous aluminosilicates.

The activity of prepared Al-substituted zeolites possessing the same topology/crystals in tetrahydropyranylation of 1-propanol was found enhancing with increasing total concentration of incorporated acid centers.

The developed methods of stabilization/alumination may extend the practical application of germanosilicate zeolites, which have high potential for application in catalysis but limited hydrothermal stability. In addition, there exists the possibility of easy recovering of Ge from acidic solution applying one of the methods proposed in Refs.[35].

Experimental Section

Synthesis of Zeolites. Samples of **ITH**, **IWW**, and **UTL** were prepared following the literature procedures[6, 22b, 24, 36] using hexamethonium (HM), N,N,N',N'-tetramethyl-1,6-hexanediamine (TMHDA), 1,5-bis(methylpyrrolidinium)-pentane (MPP), and (6R,10S)-6,10-dimethyl-5-azoniaspiro[4,5]decane (DMAD) cations as structure directing agents.

For Ge-poor **ITH** (Si/Ge = 13.3 according to chemical analysis), germanium oxide (GeO_2, 99.99 %, Aldrich) was first dissolved in a 1 M solution of HM dihydroxide followed by the addition of tetraethyl orthosilicate (TEOS, 98 %, Aldrich). The mixture was stirred at room temperature until water/ethanol was evaporated. Resulting in a gel with the composition 0.90 SiO_2 : 0.09 GeO_2 : 0.25 HM : 5 H_2O. This was

transferred into a Teflon-lined autoclave and heated at 175 °C for 14 days under slow stirring (60 rpm).[24]

Ge-rich **ITH** (Si/Ge = 2.3 according to chemical analysis) was crystallized using TMHDA as the structure-directing agent in the presence of fluorine anions according to Ren et al.[36] The synthetic suspension with the composition 0.5 SiO_2 : 0.5 GeO_2 : 7 TMHDA : 1.4 HF : 44 H_2O was then heated at 175 °C for 6 days under static conditions.

IWW samples were prepared using MPP dihydroxide as the SDA according to Ref.[6] A gel composition of (1-x) SiO_2 : x GeO_2 : 0.25 MPP : 10 H_2O was achieved, where x = 0.33 for Ge-rich **IWW** (Si/Ge = 2.9 according to chemical analysis) and x = 0.2 for Ge-poor **IWW** (Si/Ge = 7.2 according to chemical analysis), respectively. The reaction mixture was then heated at 175 °C for 7 days.

UTL samples were prepared according to Ref.[22b] by the crystallization of a gel with the composition of (1-x) SiO_2 : x GeO_2 : 0.25 DMAD : 30 H_2O at 175 °C for 6 days under agitation (60 rpm), where x = 0.33 for Ge-rich **UTL** (Si/Ge = 3.8 according to chemical analysis) and x = 0.17 for Ge-poor **UTL** (Si/Ge = 6.0 according to chemical analysis), respectively.

The solid products of hydrothermal synthesis were separated by filtration, washed out with distilled water, and dried overnight at 95 °C.

Obtained zeolites were designated as *ITH-y, IWW-y, UTL-y*, where y is Si/Ge ratio in the sample.

Post-synthesis treatment of calcined zeolites. Before the treatment, germanosilicate zeolites under investigation were calcined according to Ref.[22b, 36-37] **IWW**, **UTL** and Ge-poor **ITH** samples were calcined at 550 °C, while Ge-rich **ITH** was calcined at 650 °C for 6 h with a temperature ramp of 1 °C·min^{-1}.

Procedure 1 (Scheme 1). 0.5 g of calcined zeolite was treated with 50 mL of 1 M $Al(NO_3)_3$ solution at 80 °C for 24 h. The aluminated samples were subsequently filtrated and washed sequentially with 0.01 M HCl and deionized water and designated as *calcZeolite-y/Al*.

Procedure 2 (Scheme 1). 0.5 g of calcined zeolite was treated with 50 mL of ethanolic 1 M HCl solution. Under stirring, an additional Si source was added into the mixture (1 mmol of TEOS per 1 gram of zeolite[17]). The mixture was stirred for 0.5 h at room temperature, then transferred to Teflon-lined autoclaves and heated at 170 °C for 24 h. After the treatment, the zeolites were filtered and washed sequentially with ethanol and water, air-dried at room temperature before being subjected to alumination at 80 °C for 24 h. The aluminated samples were subsequently filtrated and washed with 0.01 M HCl and deionized water and designated as *calcZeolite-y/HCl+TEOS/Al*.

Post-synthesis treatment of as-made zeolites.

Procedure 3 (Scheme 1). The as-made zeolite was treated as described in Procedure 1. The samples were designated as *asZeolite-y/Al*.

Procedure 4 (Scheme 1). 0.5 g of as-made zeolite was treated with 50 mL of 1 M HCl solution. The mixture was stirred for 0.5 h at ambient temperature and then transferred to Teflon-lined autoclaves and heated at 170 °C for 24 h. After the treatment, the zeolites were washed with water and air-dried at room temperature. The dried samples were then subjected to alumination with 50 mL of 1 M $Al(NO_3)_3$ solution at 80 °C for 24 h. The samples were designated as *asZeolite-y/HCl/Al*.

Procedure 5 (Scheme 1). As-made zeolite was treated as described in Procedure 2. The samples were designated as *asZeolite-y/HCl+TEOS/Al*. The aluminated samples were subsequently filtered and washed with 0.01 M HCl and deionized water before being calcined at 550 – 650 °C, for 6 h with a temperature ramp of 1 °C·min^{-1} according to Ref.[22b, 36-37] to remove organic SDA.

Hydrolytic stability test. Calcined zeolites were hydrolyzed in a 0 – 0.01 M solution of nitric acid at 25 °C for 24 h with a w/w ratio 1/100. The hydrolyzed material was isolated by centrifugation, washed out with deionized water and dried at 25 °C. Zeolites, treated with 0.01 M HNO_3 were designated as *calcZeolite-y/HNO_3*.

Hydrothermal stability test. Calcined zeolites were treated in water at 100 °C for 24 h with a w/w ratio 1/100. The hydrolyzed material was isolated by centrifugation and dried at 25 °C.

Characterization. The crystallinity of all samples under investigation was determined by X-ray powder diffraction (XRD) using a Bruker AXS-D8 Advance diffractometer with a graphite monochromator and a position sensitive detector (Våntec-1) using CuKα radiation in Bragg-Brentano geometry at a scan rate of 0.25° 2θ min-1.

The concentration of Al, Ge and Si was determined by energy dispersive X-ray spectroscopy (EDX) on a Jeol JSM 5600 instrument.

Nitrogen adsorption/desorption isotherms were measured using an ASAP 2020 (Micromeritics) static volumetric apparatus at –196 °C. Prior to the sorption measurements, all samples were degassed with a turbo molecular pump at 300 °C for 8 h. Micropore size distribution was evaluated using the NLDFT method (Ar on oxides at 87 K kernel) based on the data collected by Ar adsorption at –186 °C.

The size and morphology of the zeolite crystals were examined by scanning electron microscopy (SEM, JEOL JSM-5500LV microscope). For these measurements the crystals were coated with a thin layer of platinum (~ 10 nm) in a BAL-TEC SCD-050 instrument.

Solid-state ^{27}Al NMR spectra were obtained using a Bruker Advance III spectrometer, equipped with a 9.4 T wide-bore superconducting magnet (1H Larmor frequency of 400.13 MHz). The samples were packed into a conventional 4 mm zirconia rotor and rotated at a MAS rate of 12.5 kHz using a Bruker 4 mm HFXY probe. A pulse of 1.5 μs (ν1 ≈ 100 kHz) was applied. Signal averaging was carried out for 200 transients with a repeat interval of 2 s. Spectra were referenced to 1.1 M $Al(NO_3)_3$ in D_2O using solid $Al(acac)_3$ (δ_{iso} = 0 ppm, centre of gravity = –4.2 ppm at 9.4 T) as a secondary reference.

The concentration of Lewis (cL) and Brønsted (cB) acid sites was determined after adsorption of d_3-acetonitrile (ACN) by FTIR spectroscopy using a Nicolet Protégé 460 Magna with a transmission DTGS detector. The zeolites were pressed into self-supporting wafers with a density of 8.0 – 12 mg cm^{-2} and activated in situ at T = 450 °C and p = 5·10–5 Torr for 4 h. ACN adsorption was carried out at ambient temperature for 30 min at a partial pressure of 5 Torr, followed by desorption for 20 min at the same temperature. Before adsorption ACN was degassed by freezing-pump-thaw cycles. All spectra were recorded with a resolution of 4 cm^{-1} by collecting 128 scans for a single spectrum at room temperature. Spectra were recalculated using a wafer density of 10 mg cm^{-2}. Concentration of c_L and c_B were evaluated from the integral intensities of bands at 2323 cm^{-1} (c_L) and at 2294 cm^{-1} (c_B) using extinction coefficients, ε(L) = 3.6 cm μmol^{-1}, and ε(B) = 2.05 cm μmol^{-1}.[38]

Tetrahydropyranylation of 1-propanol.

The catalytic experiments were performed in the liquid phase under atmospheric pressure at room temperature (25 °C) in a multi-experiment workstation Star-Fish (Radleys Discovery Technologies). Before using, the catalyst (100 mg) was activated at 450 °C for 120 min at a rate of

10 °C/min. Typically, 1-propanol (9 mmol), mesitylene (0.2 g; internal standard), hexane (10 mL, solvent) and the catalyst (100 mg) were added to a two-necked vessel equipped with a thermometer. DHP (15 mmol) was then added to the vessel. Samples of the reaction mixture were taken periodically and analyzed by using Agilent 6850 GC equipped a polar DB-WAX column (length 20 m, diameter 0.180 mm, and film thickness 0.3 μm) and flame ionization detector.

The reaction product was identified by using Thermo Finnigan Focus DSQ II Single Quadrupole GC/MS.

Acknowledgements

We acknowledge the valuable input from Dr Daniel Dawson and the University of St. Andrews Solid state NMR service. M.S. thanks the Czech Science Foundation for the support of the Project 14-30898P. R.E.M. thanks the EPSRC for funding through grant EP/K025112/1.

Keywords: alumination • germanosilicate zeolites • **ITH** • **IWW** • **UTL**

[1] a) A. Corma, M. T. Navarro, F. Rey, J. Rius, S. Valencia, *Angew. Chem., Int. Ed.* **2001**, *40*, 2277-2280; b) G. Sastre, J. A. Vidal-Moya, T. Blasco, J. Rius, J. L. Jordá, M. T. Navarro, F. Rey, A. Corma, *Angew. Chem., Int. Ed.* **2002**, *41*, 4722-4726; c) J. Jiang, J. Yu, A. Corma, *Angew. Chem., Int. Ed.* **2010**, *49*, 3120-3145; d) A. Corma, M. J. Diaz-Cabanas, J. Jiang, M. Afeworki, D. L. Dorset, S. L. Soled, K. G. Strohmaier, *Proc. Natl. Acad. Sci. U. S. A.* **2010**, *107*, 13997-14002; e) J. Jiang, J. L. Jorda, M. J. Diaz-Cabanas, J. Yu, A. Corma, *Angew. Chem., Int. Ed.* **2010**, *49*, 4986-4988.

[2] T. Conradsson, M. S. Dadachov, X. D. Zou, *Microporous Mesoporous Mater.* **2000**, *41*, 183-191.

[3] H. L. Li, O. M. Yaghi, *J. Am. Chem. Soc.* **1998**, *120*, 10569-10570.

[4] R. Castañeda, A. Corma, V. Fornes, F. Rey, J. Rius, *J. Am. Chem. Soc.* **2003**, *125*, 7820-7821.

[5] D. L. Dorset, K. G. Strohmaier, C. E. Kliewer, A. Corma, M. J. Díaz-Cabañas, F. Rey, C. J. Gilmore, *Chem. Mater.* **2008**, *20*, 5325-5331.

[6] A. Corma, F. Rey, S. Valencia, J. L. Jorda, J. Rius, *Nat. Mater.* **2003**, *2*, 493-497.

[7] J. Sun, C. Bonneau, A. Cantin, A. Corma, M. J. Diaz-Cabanas, M. Moliner, D. Zhang, M. Li, X. Zou, *Nature* **2009**, *458*, 1154-1157.

[8] a) J. L. Paillaud, B. Harbuzaru, J. Patarin, N. Bats, *Science* **2004**, *304*, 990-992; b) A. Corma, M. J. Diaz-Cabanas, F. Rey, S. Nicolopoulas, K. Boulahya, *Chem. Commun. (Cambridge, U. K.)* **2004**, 1356-1357.

[9] A. Corma, M. J. Diaz-Cabanas, J. L. Jorda, F. Rey, G. Sastre, K. G. Strohmaier, *J. Am. Chem. Soc.* **2008**, *130*, 16482-16483.

[10] M. Dodin, J.-L. Paillaud, Y. Lorgouilloux, P. Caullett, E. Elkaim, N. Bats, *J. Am. Chem. Soc.* **2010**, *132*, 10221-10223.

[11] a) M. O'Keeffe, O. M. Yaghi, *Chem. Eur. J.* **1999**, *5*, 2796-2801; b) T. Blasco, A. Corma, M. J. Diaz-Cabanas, F. Rey, J. A. Vidal-Moya, C. M. Zicovich-Wilson, *J. Phys. Chem. B* **2002**, *106*, 2634-2642; c) G. Sastre, A. Pulido, A. Corma, *Microporous Mesoporous Mater.* **2005**, *82*, 159-163.

[12] a) W. J. Roth, O. V. Shvets, M. Shamzhy, P. Chlubna, M. Kubu, P. Nachtigall, J. Čejka, *J. Amer. Chem. Soc.* **2011**, *133*, 6130-6133; b) M. Mazur, P. S. Wheatley, M. Navarro, W. J. Roth, M. Položij, A. Mayoral, P. Eliášová, P. Nachtigall, J. Čejka, R. E. Morris, *Nat. Chem.* **2016**, *8*, 58-62.

[13] P. Chlubná-Eliášová, Y. Tian, A. B. Pinar, M. Kubů, J. Čejka, R. E. Morris, *Angew. Chem., Int. Ed.* **2014**, *53*, 7042-7052.

[14] L. Tang, L. Shi, C. Bonneau, J. Sun, H. Yue, A. Ojuva, B.-L. Lee, M. Kritikos, R. G. Bell, Z. Bacsik, J. Mink, X. Zou, *Nat. Mater.* **2008**, *7*, 381-385.

[15] F. Gao, M. Jaber, K. Bozhilov, A. Vicente, C. Fernandez, V. Valtchev, *J. Am. Chem. Soc.* **2009**, *131*, 16580-16586.

[16] L. Burel, N. Kasian, A. Tuel, *Angew. Chem., Int. Ed.* **2014**, *53*, 1360-1363.

[17] H. Xu, J.-g. Jiang, B. Yang, L. Zhang, M. He, P. Wu, *Angew. Chem., Int. Ed.* **2014**, *53*, 1355-1359.

[18] a) M. Shamzhy, F. S. d. O. Ramos, *Catal. Today* **2015**, *243*, 76-84; b) P. Eliášová, M. Opanasenko, P. S. Wheatley, M. Shamzhy, M. Mazur, P. Nachtigall, W. J. Roth, R. E. Morris, J. Čejka, *Chem. Soc. Rev.* **2015**, *44*, 7177-7206.

[19] X. Liu, U. Ravon, F. Bosselet, G. Bergeret, A. Tuel, *Chem. Mater.* **2012**, *24*, 3016-3022.

[20] J. A. Vidal-Moya, T. Blasco, F. Rey, A. Corma, M. Puche, *Chem. Mater.* **2003**, *15*, 3961-3963.

[21] M. Shamzhy, M. Opanasenko, Y. Tian, K. Konysheva, O. Shvets, R. E. Morris, J. Čejka, *Chem. Mater.* **2014**, *26*, 5789-5798.

[22] a) O. V. Shvets, M. V. Shamzhy, P. S. Yaremov, Z. Musilova, D. Prochazkova, J. Čejka, *Chem. Mater.* **2011**, *23*, 2573-2585; b) M. V. Shamzhy, O. V. Shvets, M. V. Opanasenko, P. S. Yaremov, L. G. Sarkisyan, P. Chlubna, A. Zukal, V. R. Marthala, M. Hartmann, J. Čejka, *J. Mater. Chem.* **2012**, *22*, 15793-15803.

[23] N. Kasian, A. Tuel, E. Verheyen, C. E. A. Kirschhock, F. Taulelle, J. A. Martens, *Chem. Mater.* **2014**, *26*, 5556-5565.

[24] R. Castañeda, A. Corma, V. Fornes, J. Martinez-Triguero, S. Valencia, *J. Catal.* **2006**, *238*, 79-87.

[25] R. L. Smith, P. Eliasova, M. Mazur, M. P. Attfield, J. Cejka, M. W. Anderson, *Chem. Eur. J.* **2014**, *20*, 10446-10450.

[26] a) C. Y. Chen, S. I. Zones, US 6,468,501, **2002**; b) C.-Y. Chen, S. I. Zones, in *Zeolites and Catalysis*, Wiley-VCH Verlag GmbH & Co. KGaA, **2010**, pp. 155-170.

[27] M. Kosmulski, *Chemical Properties of Material Surfaces*, CRC Press, **2001**.

[28] L. Tosheva, N. Mahé, V. Valtchev, in *Stud. Surf. Sci. Catal., Vol. 170* (Eds.: Z. G. J. C. Ruren Xu, Y. Wenfu), Elsevier, **2007**, pp. 616-621.

[29] P. S. Wheatley, P. Chlubná-Eliášová, H. Greer, W. Zhou, V. R. Seymour, D. M. Dawson, S. E. Ashbrook, A. B. Pinar, L. B. McCusker, M. Opanasenko, J. Čejka, R. E. Morris, *Angew. Chem., Int. Ed.* **2014**, *53*, 13210-13214.

[30] in *Multinuclear Solid-State NMR of Inorganic Materials, Vol. 6* (Eds.: J. D. M. Kenneth, E. S. Mark), Pergamon, **2002**, pp. 271-330.

[31] R. E. Morris, J. Čejka, *Nat. Chem.* **2015**, *7*, 381-388.

[32] M. Shamzhy, M. Opanasenko, Y. Tian, K. Konysheya, O. Shvets, R. E. Morris, J. Čejka, *Chemistry of Materials* **2014**, *26*, 5789-5798.

[33] R. Szostak, *Molecular sieves: principles of synthesis and identification*, Springer, **1998**.

[34] C. Martinez, D. Verboekend, J. Perez-Ramirez, A. Corma, *Catal. Sci. Tech.* **2013**, *3*, 972-981.

[35] a) A. Hernandez-Exposito, J. M. Chimenos, A. I. Fernandez, O. Font, X. Querol, P. Coca, F. G. Pena, *Chem. Eng. J. (Lausanne)* **2006**, *118*, 69-75; b) K. A. Matis, P. Mavros, *Sep. Purif. Methods* **1991**, *20*, 1-48; c) J. P. Marco-Lozar, D. Cazorla-Amoros, A. Linares-Solano, *Carbon* **2007**, *45*, 2519-2528; d) F. J. S. Menendez, F. M. S. Menendez, A. de la Cuadra Herrera, F. A. Tamargo, L. P. Lorenzo, M. R. Valcarcel, V. A. Fernandez, in *US 4,886,648* (Ed.: US 4, 648), US 4,886,648, US 4,886,648, **1989**.

[36] X. Ren, J. Liu, Y. Li, J. Yu, R. Xu, *J. Porous Mater.* **2013**, *20*, 975-981.

[37] G. Sastre, A. Pulido, R. Castañeda, A. Corma, *J. Phys. Chem. B* **2004**, *108*, 8830-8835.

[38] B. Wichterlová, Z. Tvarůžková, Z. Sobalík, P. Sarv, *Microporous Mesoporous Mater.* **1998**, *24*, 223-233.

Entry for the Table of Contents (Please choose one layout)

FULL PAPER

The stabilization of the extra-large pore zeolite **UTL** by the partial post-synthesis substitution of Ge for Si and Al is reported for the first time.

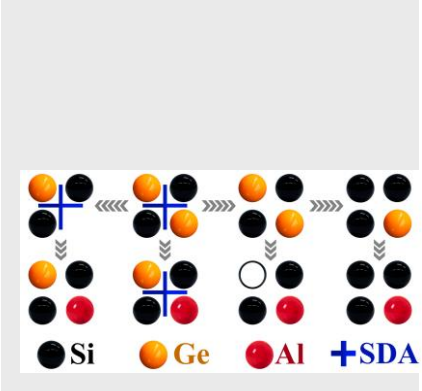

Mariya V. Shamzhy, Pavla Eliašová, Dana Vitvarová, Maksym V. Opanasenko, Daniel S. Firth, Russell E. Morris*

Page No. – Page No.

Post-synthesis stabilization of germanosilicate zeolites ITH, IWW and UTL by substitution of Ge for Al